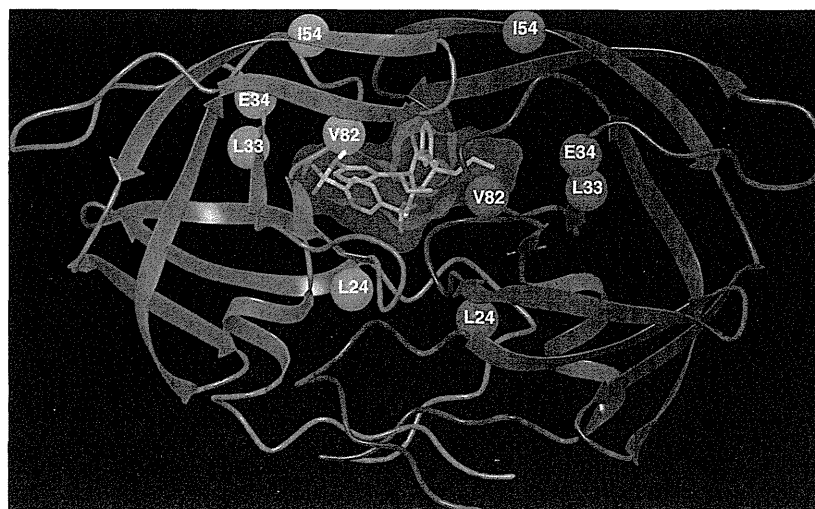


**FIG 6** Impact of amino acid substitutions that appeared in TPV selection on TPV's dimerization inhibition. COS7 cells were cotransfected with a pair of clones, HIV<sub>NL4-3</sub><sup>CFP</sup> and pHIV<sub>NL4-3</sub><sup>YFP</sup>, carrying E34D (cHIV<sub>NL4-3</sub><sup>E34D</sup>), L63P (cHIV<sub>NL4-3</sub><sup>L63P</sup>), A71V (cHIV<sub>NL4-3</sub><sup>A71V</sup>), K45I (cHIV<sub>NL4-3</sub><sup>K45I</sup>), or V82L (cHIV<sub>NL4-3</sub><sup>V82L</sup>). COS7 cells were further cultured in the continuous presence of 1 or 10  $\mu$ M TPV, and CFP<sup>AB</sup> ratios were determined at the conclusion of the 3-day period of culture. \*, not significant; \*\*,  $P < 0.05$ .

ent study were as sensitive to TPV as the wild-type clinical HIV-1 isolate (HIV<sub>104pre</sub>) (Table 1), although they were moderately to highly resistant to 5 other approved PIs, including SQV, IDV, APV, LPV, and ATV (Table 1). However, the TPV-selected HIV-1 variants became highly resistant to TPV and were much more resistant to all 5 PIs without specific resistance mutations to each PI, as previously reported (9). It is noteworthy that HIV<sub>11MIX</sub><sup>P10</sup> remained relatively susceptible to DRV with an IC<sub>50</sub> of 0.034  $\mu$ M (Table 2).

In HIV<sub>11MIX</sub><sup>P10</sup> and 3 of the 4 TPV-selected clinical strains (HIV<sub>B</sub><sup>P10</sup>, HIV<sub>C</sub><sup>P15</sup>, and HIV<sub>TM</sub><sup>P15</sup>), two amino acid substitutions, I54V and V82T, which reportedly contribute to decreased TPV susceptibility (33) were identified to be major TPV resistance-associated amino acid substitutions (Fig. 3A and B). Since HIV<sub>B</sub> readily started propagating under TPV selection (Fig. 2) and ac-

quired V82T by passage 10 (HIV<sub>B</sub><sup>P10</sup>), we also examined the impact of I54V and I54V/V82T upon TPV's protease dimerization inhibition activity with the genetic background of cHIV<sub>B</sub> (Fig. 4B). Neither cHIV<sub>B</sub><sup>I54V</sup> nor cHIV<sub>B</sub><sup>I54V/V82T</sup> had any further impact on TPV's dimerization inhibition activity (Fig. 4B). Nevertheless, the susceptibility of cHIV<sub>B</sub><sup>I54V</sup> and cHIV<sub>B</sub><sup>I54V/V82T</sup> was significantly decreased (Table 3), even though the I54V and V82T mutations did not confer resistance to TPV in HIV<sub>NL4-3</sub> (Table 3). These findings are perhaps in line with multiple reports that single amino acid substitutions in HIV-1 protease do not significantly change viral sensitivity to PIs (16). It is presumed that these two amino acid substitutions ultimately affect HIV-1's susceptibility to TPV only when they are present with other subsequently acquired amino acid substitutions. Figure 7 shows the mature dimerized HIV-1 protease in complex with TPV and the locations



**FIG 7** The mature dimerized HIV-1 protease in complex with TPV. The locations of amino acid substitutions L24M, L33I/F, E34D, I54V, and V82T associated with HIV TPV resistance are shown.

of the amino acid substitutions (L24M, L33I/F, E34D, I54V, and V82T) associated with HIV TPV resistance.

Rhee et al. reported that the F53L mutation is slightly related to HIV's increased susceptibility to TPV (33). In the present study, HIV<sub>EV</sub> contained F53L (see Fig. S1 in the supplemental material) and had increased sensitivity to TPV (IC<sub>50</sub>, 0.066  $\mu$ M) compared to the wild-type HIV (HIV<sub>104pre</sub>; IC<sub>50</sub>, 0.16  $\mu$ M). Most of HIV<sub>B</sub><sup>P0</sup> clones (16/20) contained F53L but had a sensitivity (IC<sub>50</sub>, 0.18  $\mu$ M) comparable to that of HIV<sub>104pre</sub>; however, by passage 10 under TPV selection, all the clones of HIV<sub>B</sub><sup>P10</sup> had lost F53L (Fig. 3B). These data suggest that F53L contributed to the increased sensitivity to TPV (in the case of HIV<sub>EV</sub>) and sensitivity comparable to that of HIV<sub>104pre</sub> (in the case of HIV<sub>B</sub>).

HIV<sub>C</sub>, which initially contained L24I, acquired L24M by passage 15 under TPV selection (Fig. 3B), and the L24M mutation conferred resistance to TPV on HIV<sub>C</sub> (IC<sub>50</sub>s of cHIV<sub>C</sub> and cHIV<sub>C</sub><sup>L24M</sup>, 0.9 and 2.2  $\mu$ M, respectively; Table 4). Moreover, TPV lost its protease dimerization inhibition activity when the L24M mutation was introduced into HIV<sub>NL4-3</sub> (cHIV<sub>NL4-3</sub><sup>L24M</sup>) (Fig. 4C). Nevertheless, the same cHIV<sub>NL4-3</sub><sup>L24M</sup> clone had an increased sensitivity to TPV (0.1-fold difference), as shown in Table 4. It is possible that the TPV resistance may not always be caused by the PR mutations that interfere with TPV's inhibition of dimerization and that the genetic barrier to TPV resistance via the loss of dimerization inhibition could be much lower than that for DRV. However, it is also possible that the loss of TPV's dimerization inhibition activity associated with L24M acquisition might have offset an otherwise highly increased susceptibility of HIV-1 to TPV caused by the same effect of L24M on the catalytic activity of protease. In other words, if L24M does not confer TPV resistance by reducing TPV's dimerization inhibition activity, HIV<sub>NL4-3</sub><sup>L24M</sup> could be extremely more susceptible to TPV. Thus, while L24M contributes to both the acquisition of TPV resistance of HIV<sub>C</sub> and the loss of dimerization inhibition activity of TPV, the effects of L24M apparently depend on the genetic background of the HIV-1 species. The present data suggest that the conformation of the active site in the proximity of amino acid position 24 is altered by additional amino acid substitutions, although such conformational changes remain to be elucidated.

The L33I substitution seen in HIV<sub>11MIX</sub><sup>P5</sup>, HIV<sub>11MIX</sub><sup>P10</sup>, HIV<sub>B</sub><sup>P0</sup>, and HIV<sub>B</sub><sup>P10</sup> compromised the activity of TPV to block protease dimerization with the genetic background of cHIV<sub>NL4-3</sub> (Fig. 4C). Nevertheless, cHIV<sub>B</sub> that contained L33I was as susceptible to TPV's activity against replication as cHIV<sub>NL4-3</sub> (Table 3). Moreover, neither L33I in cHIV<sub>NL4-3</sub><sup>L33I/M36I</sup> nor L33F in cHIV<sub>NL4-3</sub><sup>L33F</sup> caused significant changes in the susceptibility of cHIV<sub>NL4-3</sub> to TPV's antiviral activity (Table 3). Therefore, in order to further examine the effect of L33I in the genetic background of cHIV<sub>B</sub>, L33I was reverted to the wild-type amino acid, Ile-33, generating cHIV<sub>B</sub><sup>I33L</sup>, which was also as susceptible to TPV's anti-HIV activity as cHIV<sub>NL4-3</sub>. However, when L33I was reverted to Ile-33 in cHIV<sub>B</sub><sup>I54V</sup> and cHIV<sub>B</sub><sup>I54V/V82T</sup>, generating cHIV<sub>B</sub><sup>I33L/I54V</sup> and cHIV<sub>B</sub><sup>I33L/I54V/V82T</sup>, respectively, they proved to be less resistant to TPV's anti-HIV activity (Table 3). These data suggest that although L33I is not significantly associated with the acquisition of TPV resistance in cHIV<sub>B</sub>, L33I does increase the level of resistance of cHIV<sub>B</sub><sup>I54V</sup> and cHIV<sub>B</sub><sup>I54V/V82T</sup> to TPV. The reason why the conversion of Ile-33 to Leu-33 did not alter the IC<sub>50</sub> between cHIV<sub>B</sub> and cHIV<sub>B</sub><sup>I33L</sup> (Table 3) could be that the p24 Gag protein production system was not sensitive enough to detect the poten-

tial difference in the IC<sub>50</sub>s. It is also possible that the activity of TPV to block protease dimerization may not significantly contribute to the overall anti-HIV activity of TPV.

In the present study, when L33I was introduced into cHIV<sub>NL4-3</sub> (generating cHIV<sub>NL4-3</sub><sup>L33I</sup>), cHIV<sub>NL4-3</sub><sup>L33I</sup> had no replicative activity, while further addition of M36I (generating cHIV<sub>NL4-3</sub><sup>L33I/M36I</sup>) restored the replicative activity (Table 3). In this regard, we have previously reported that HIV-1 can acquire substantial drug resistance with initial amino acid substitutions, sacrificing some replication ability; however, the same virus population subsequently acquires additional substitutions and becomes optimally replication competent (26). On the other hand, the introduction of L24I and L24M into cHIV<sub>NL4-3</sub> (generating cHIV<sub>NL4-3</sub><sup>L24I</sup> and cHIV<sub>NL4-3</sub><sup>L24M</sup>) rendered cHIV<sub>NL4-3</sub> more susceptible to TPV, with the IC<sub>50</sub> difference being 13.5- and 9.3-fold, respectively, relative to the IC<sub>50</sub> of cHIV<sub>NL4-3</sub> (Table 4). Such a case has also been well-known. For example, the M184V substitution alone renders HIV-1 highly resistant to lamivudine, but on the contrary, M184V makes HIV-1 highly susceptible to zidovudine (25). It is presumed that such an amino acid substitution(s) alters viral enzyme structures critical for the interactions of the enzyme with substrates and drugs; however, the mechanisms by which such profound changes in HIV replicability and drug sensitivity occur largely remain to be elucidated.

Since the introduction of L33I completely abrogated the replication of HIV<sub>NL4-3</sub> (Table 3), we introduced L33F (generating cHIV<sub>NL4-3</sub><sup>L33F</sup>), which has been identified in HIV-1 clinically exposed to TPV (24, 28). In cHIV<sub>NL4-3</sub><sup>L33F</sup>, TPV failed to block protease dimerization (Fig. 4C); however, cHIV<sub>NL4-3</sub><sup>L33F</sup> was as TPV sensitive as cHIV<sub>NL4-3</sub> (Table 3). Thus, we presumed that the loss of dimerization inhibition by TPV did not significantly contribute to cHIV<sub>NL4-3</sub><sup>L33F</sup>'s overall sensitivity to TPV. It is possible that in cHIV<sub>NL4-3</sub><sup>L33F</sup>, L33F confers an increased sensitivity to TPV, overriding the loss of TPV's dimerization inhibition and rendering cHIV<sub>NL4-3</sub><sup>L33F</sup> as sensitive to TPV as wild-type cHIV<sub>NL4-3</sub>. Therefore, we finally propagated three recombinant clones, cHIV<sub>NL4-3</sub>, cHIV<sub>NL4-3</sub><sup>L33F</sup>, and cHIV<sub>NL4-3</sub><sup>I54V/V82T</sup>, in the presence of increasing concentrations of TPV, in an attempt to examine whether these substitutions help the virus rapidly acquire resistance to TPV. The acquisition of TPV resistance of cHIV<sub>NL4-3</sub><sup>L33F</sup> was fairly delayed compared to that of cHIV<sub>NL4-3</sub><sup>I54V/V82T</sup>, followed by cHIV<sub>NL4-3</sub>, suggesting that the presence of I54V/V82T not only renders certain HIV-1 strains (such as HIV<sub>B</sub>) resistant to TPV but also predisposes cHIV<sub>NL4-3</sub> to more readily develop resistance to TPV. The determination of nucleic acid sequences revealed that at passage 10 cHIV<sub>NL4-3</sub><sup>I54V/V82T</sup> had acquired three new substitutions, E34D, L63P, and A71V. At passage 20, cHIV<sub>NL4-3</sub> had acquired two relatively unique amino acid substitutions, K45I and V82L. Thus, we again examined whether these five substitutions caused any changes in the ability of TPV to block protease dimerization. The FRET-based HIV-1 expression assay using newly generated recombinant protease with each of the substitutions showed that only E34D compromised TPV's protease dimerization inhibition activity. These data again confirmed our present interpretation, in that although the loss of TPV's protease dimerization inhibition due to the E34D substitution is involved in the acquisition of TPV resistance of HIV, other amino acid substitutions (such as L63P, A71V, K45I, and V82L) are not related to the protease susceptibility of TPV's dimerization inhibition but are associated with the acquisition of viral resistance to TPV. In this regard, HIV<sub>A</sub> did not

TABLE 5 Summary of impacts of amino acid substitutions in protease on TPV's protease dimerization inhibition and anti-HIV activity

Genetic background	Reduction of TPV's activity to inhibit	Amino acid substitution in PR											
		L24I	L24 M	L33I	L33F	E34D	K45I	I54V	L63P	A71V	V82L	V82T	I54V/V82T
cHIV <sub>NL4-3</sub>	Protease dimerization	—	+	+	+	+	—	—	—	—	—	—	—
	HIV replication	E <sup>a</sup>	E	—	—	ND <sup>b</sup>	ND	—	ND	ND	—	—	—
cHIV <sub>B</sub>	Protease dimerization	ND	ND	+	ND	ND	ND	—	ND	ND	ND	—	—
	HIV replication	ND	ND	+ <sup>c</sup>	ND	ND	ND	+	ND	ND	ND	+	+
cHIV <sub>C</sub>	Protease dimerization	ND	ND	ND	ND	ND	ND	ND	ND	ND	ND	ND	ND
	HIV replication	ND	+	ND	ND	ND	ND	ND	ND	ND	ND	+	ND

<sup>a</sup> E, TPV's activity to inhibit HIV replication was enhanced with certain genetic backgrounds.

<sup>b</sup> ND, not determined.

<sup>c</sup> When the L33I mutation exists with the genetic background of cHIV<sub>B</sub> carrying I54V or I54V/V82T, L33I reduces the antiviral activity of TPV.

become predominant by passage 5 under TPV selection (Fig. 3A), although HIV<sub>A</sub> originally had both I54V and V82T before TPV selection (see Fig. S1 in the supplemental material), suggesting that the acquisition of high levels of resistance to TPV requires the acquisition of mutations associated with not only the blockage of replicative activity but also dimerization inhibition activity.

It is of note that the altered susceptibility of protease to TPV's dimerization inhibition activity differs substantially with the genetic background of HIV. The impact of amino acid substitutions in protease on TPV's protease dimerization inhibition activity and antiviral activity is summarized in Table 5.

Importantly, TPV's activity to block protease dimerization is compromised mostly with a single amino acid substitution, while the loss of DRV's ability to block protease dimerization requires as many as 4 amino acid substitutions (20). In addition, the activity of TPV to block protease dimerization *per se* is significantly less potent than that of DRV. These data together should explain why the genetic barrier of TPV against viral resistance is substantially lower than that of DRV. The present data on TPV as well as thus far published data on DRV (20, 21) demonstrate that the inhibition of protease dimerization contributes to the overall anti-HIV-1 activity of TPV and DRV, and it is hoped that agents with further potent activity to block protease dimerization can be developed.

## ACKNOWLEDGMENTS

This work was supported in part by a grant for global education and a research center aiming at the control of AIDS (Global Center of Excellence supported by Monbu-Kagakusho), a grant for the promotion of AIDS research from the Ministry of Health, Welfare, and Labor of Japan, a grant to the Cooperative Research Project on Clinical and Epidemiological Studies of Emerging and Re-Emerging Infectious Diseases (Renkei Jigyo no. 78, Kumamoto University) of Monbu-Kagakusho, and a Grant-in-Aid for Young Scientists (B) (grant 21790527) of Monbu-Kagakusho and in part by the Intramural Research Program of Center for Cancer Research, National Cancer Institute, National Institutes of Health.

## REFERENCES

- Amano M, et al. 2007. A novel bis-tetrahydrofuranylurethane-containing nonpeptidic protease inhibitor (PI), GRL-98065, is potent against multiple-PI-resistant human immunodeficiency virus in vitro. *Antimicrob. Agents Chemother.* 51:2143–2155.
- Aoki M, et al. 2009. Non-cleavage site gag mutations in amprenavir-resistant human immunodeficiency virus type 1 (HIV-1) predispose HIV-1 to rapid acquisition of amprenavir resistance but delay development of resistance to other protease inhibitors. *J. Virol.* 83:3059–3068.
- Back NK, et al. 2000. In-vitro tipranavir susceptibility of HIV-1 isolates with reduced susceptibility to other protease inhibitors. *AIDS* 14:101–102.
- Baxter JD, et al. 2006. Genotypic changes in human immunodeficiency virus type 1 protease associated with reduced susceptibility and virologic response to the protease inhibitor tipranavir. *J. Virol.* 80:10794–10801.
- Cooper D, Zajdenverg R, Ruxrungtham K, Scherer J, Chaves R. 2006. Efficacy and safety of two doses of tipranavir/ritonavir versus lopinavir/ritonavir-based therapy in antiretroviral-naïve patients: results of BI 1182.33. *Abstr. 8th Int. Cong. Drug Ther. HIV Infect., Glasgow, Scotland.*
- De Meyer S, et al. 2005. TMC114, a novel human immunodeficiency virus type 1 protease inhibitor active against protease inhibitor-resistant viruses, including a broad range of clinical isolates. *Antimicrob. Agents Chemother.* 49:2314–2321.
- de Meyer S, et al. 2008. Resistance profile of darunavir: combined 24-week results from the POWER trials. *AIDS Res. Hum. Retroviruses* 24: 379–388.
- Dierynck I, et al. 2007. Binding kinetics of darunavir to human immunodeficiency virus type 1 protease explain the potent antiviral activity and high genetic barrier. *J. Virol.* 81:13845–13851.
- Doyon L, Tremblay S, Bourgon L, Wardrop E, Cordingley MG. 2005. Selection and characterization of HIV-1 showing reduced susceptibility to the non-peptidic protease inhibitor tipranavir. *Antiviral Res.* 68:27–35.
- Fang G, Weiser B, Visosky A, Moran T, Burger H. 1999. PCR-mediated recombination: a general method applied to construct chimeric infectious molecular clones of plasma-derived HIV-1 RNA. *Nat. Med.* 5:239–242.
- Gatanaga H, et al. 2002. Amino acid substitutions in Gag protein at non-cleavage sites are indispensable for the development of a high multiplicity of HIV-1 resistance against protease inhibitors. *J. Biol. Chem.* 277: 5952–5961.
- Ghosh AK, et al. 1998. Potent HIV protease inhibitors incorporating high-affinity P2-ligands and (R)-(hydroxyethylamino)sulfonamide isostere. *Bioorg. Med. Chem. Lett.* 8:687–690.
- Ghosh AK, et al. 1998. Structure based design: novel spirocyclic ethers as nonpeptidic P2-ligands for HIV protease inhibitors. *Bioorg. Med. Chem. Lett.* 8:979–982.
- Ghosh AK, Leshchenko S, Noetzel M. 2004. Stereoselective photochemical 1,3-dioxolane addition to 5-alkoxymethyl-2(5H)-furanone: synthesis of bis-tetrahydrofuranyl ligand for HIV protease inhibitor UIC-94017 (TMC-114). *J. Org. Chem.* 69:7822–7829.
- Harada S, Hazra R, Tamiya S, Zeichner SL, Mitsuya H. 2007. Emergence of human immunodeficiency virus type 1 variants containing the Q151M complex in children receiving long-term antiretroviral chemotherapy. *Antiviral Res.* 75:159–166.
- Henderson GJ, et al. 2012. Interplay between single resistance-associated mutations in the HIV-1 protease and viral infectivity, protease activity, and inhibitor sensitivity. *Antimicrob. Agents Chemother.* 56:623–633.
- Hsieh SM, et al. 2011. Emerging HIV-1 resistance to tipranavir and

- darunavir in patients with virological failure to first-generation protease inhibitors in Taiwan. *Int. J. STD AIDS* 22:617–620.
18. Ide K, et al. 2011. Novel HIV-1 protease inhibitors (PIs) containing a bicyclic P2 functional moiety, tetrahydropyrano-tetrahydrofuran, that are potent against multi-PI-resistant HIV-1 variants. *Antimicrob. Agents Chemother.* 55:1717–1727.
  19. Koh Y, et al. 2010. In vitro selection of highly darunavir-resistant and replication-competent HIV-1 variants by using a mixture of clinical HIV-1 isolates resistant to multiple conventional protease inhibitors. *J. Virol.* 84:11961–11969.
  20. Koh Y, et al. 2011. Loss of protease dimerization inhibition activity of darunavir is associated with the acquisition of resistance to darunavir by HIV-1. *J. Virol.* 85:10079–10089.
  21. Koh Y, et al. 2007. Potent inhibition of HIV-1 replication by novel non-peptidyl small molecule inhibitors of protease dimerization. *J. Biol. Chem.* 282:28709–28720.
  22. Koh Y, et al. 2003. Novel bis-tetrahydrofuranylurethane-containing non-peptidic protease inhibitor (PI) UIC-94017 (TMC114) with potent activity against multi-PI-resistant human immunodeficiency virus in vitro. *Antimicrob. Agents Chemother.* 47:3123–3129.
  23. Kohl NE, et al. 1988. Active human immunodeficiency virus protease is required for viral infectivity. *Proc. Natl. Acad. Sci. U. S. A.* 85:4686–4690.
  24. Larder BA, et al. 2000. Tipranavir inhibits broadly protease inhibitor-resistant HIV-1 clinical samples. *AIDS* 14:1943–1948.
  25. Larder BA, Kemp SD, Harrigan PR. 1995. Potential mechanism for sustained antiretroviral efficacy of AZT-3TC combination therapy. *Science* 269:696–699.
  26. Maeda Y, Venzon DJ, Mitsuya H. 1998. Altered drug sensitivity, fitness, and evolution of human immunodeficiency virus type 1 with pol gene mutations conferring multi-dideoxynucleoside resistance. *J. Infect. Dis.* 177:1207–1213.
  27. Mitsuya Y, Liu TF, Rhee SY, Fessel WJ, Shafer RW. 2007. Prevalence of darunavir resistance-associated mutations: patterns of occurrence and association with past treatment. *J. Infect. Dis.* 196:1177–1179.
  28. Naeger LK, Struble KA. 2007. Food and Drug Administration analysis of tipranavir clinical resistance in HIV-1-infected treatment-experienced patients. *AIDS* 21:179–185.
  29. Panel on Antiretroviral Guidelines for Adults and Adolescents. 2012. Guidelines for the use of antiretroviral agents in HIV-1-infected adults and adolescents. U.S. Department of Health and Human Services, Washington, DC. <http://aidsinfo.nih.gov/contentfiles/lvguidelines/AdultandAdolescentGL.pdf>. Accessed 13 August 2012.
  30. Poppe SM, et al. 1997. Antiviral activity of the dihydropyrene PNU-140690, a new nonpeptidic human immunodeficiency virus protease inhibitor. *Antimicrob. Agents Chemother.* 41:1058–1063.
  31. Poveda E, et al. 2010. Drug resistance mutations in HIV-infected patients in the Spanish drug resistance database failing tipranavir and darunavir therapy. *Antimicrob. Agents Chemother.* 54:3018–3020.
  32. Poveda E, et al. 2006. Successful rescue therapy with darunavir (TMC114) in HIV-infected patients who have failed several ritonavir-boosted protease inhibitors. *AIDS* 20:1558–1560.
  33. Rhee SY, et al. 2010. HIV-1 protease mutations and protease inhibitor cross-resistance. *Antimicrob. Agents Chemother.* 54:4253–4261.
  34. Schapiro JM, et al. 2010. Improving the prediction of virological response to tipranavir: the development and validation of a tipranavir-weighted mutation score. *Antivir. Ther.* 15:1011–1019.
  35. Shirasaka T, et al. 1993. Changes in drug sensitivity of human immunodeficiency virus type 1 during therapy with azidothymidine, dideoxycytidine, and dideoxyinosine: an in vitro comparative study. *Proc. Natl. Acad. Sci. U. S. A.* 90:562–566.
  36. Tamiya S, Mardy S, Kavlick MF, Yoshimura K, Mistuya H. 2004. Amino acid insertions near Gag cleavage sites restore the otherwise compromised replication of human immunodeficiency virus type 1 variants resistant to protease inhibitors. *J. Virol.* 78:12030–12040.
  37. Temesgen Z, Feinberg J. 2007. Tipranavir: a new option for the treatment of drug-resistant HIV infection. *Clin. Infect. Dis.* 45:761–769.
  38. Van Marck H, et al. 2009. The impact of individual human immunodeficiency virus type 1 protease mutations on drug susceptibility is highly influenced by complex interactions with the background protease sequence. *J. Virol.* 83:9512–9520.
  39. Wlodawer A, et al. 1989. Conserved folding in retroviral proteases: crystal structure of a synthetic HIV-1 protease. *Science* 245:616–621.
  40. Yoshimura K, et al. 2002. A potent human immunodeficiency virus type 1 protease inhibitor, UIC-94003 (TMC-126), and selection of a novel (A28S) mutation in the protease active site. *J. Virol.* 76:1349–1358.
  41. Yoshimura K, et al. 1999. JE-2147: a dipeptide protease inhibitor (PI) that potentially inhibits multi-PI-resistant HIV-1. *Proc. Natl. Acad. Sci. U. S. A.* 96:8675–8680.



## Substituent effects on P2-cyclopentyltetrahydrofuranyl urethanes: Design, synthesis, and X-ray studies of potent HIV-1 protease inhibitors

Arun K. Ghosh<sup>a,\*</sup>, Bruno D. Chapsal<sup>a</sup>, Melinda Steffey<sup>a</sup>, Johnson Agniswamy<sup>b</sup>, Yuan-Fang Wang<sup>b</sup>, Masayuki Amano<sup>c</sup>, Irene T. Weber<sup>b</sup>, Hiroaki Mitsuya<sup>c,d</sup>

<sup>a</sup> Department of Chemistry and Department of Medicinal Chemistry, Purdue University, West Lafayette, IN 47907, USA

<sup>b</sup> Department of Biology, Molecular Basis of Disease, Georgia State University, Atlanta, GA 30303, USA

<sup>c</sup> Departments of Hematology and Infectious Diseases, Kumamoto University Graduate School of Medical and Pharmaceutical Sciences, Kumamoto 860-8556, Japan

<sup>d</sup> Experimental Retrovirology Section, HIV and AIDS Malignancy Branch, National Cancer Institute, National Institutes of Health, Bethesda, MD 20892, USA

### ARTICLE INFO

#### Article history:

Received 28 December 2011

Accepted 17 January 2012

Available online 2 February 2012

#### Keywords:

HIV-1 protease inhibitors

P2 ligand

Drug resistance

Design and synthesis

X-ray crystal structure

### ABSTRACT

The design, synthesis, and biological evaluation of novel C3-substituted cyclopentyltetrahydrofuranyl (Cp-THF)-derived HIV-1 protease inhibitors are described. Various C3-functional groups on the Cp-THF ligand were investigated in order to maximize the ligand-binding site interactions in the flap region of the protease. Inhibitors **3c** and **3d** have displayed the most potent enzyme inhibitory and antiviral activity. Both inhibitors have maintained impressive activity against a panel of multidrug resistant HIV-1 variants. A high-resolution X-ray crystal structure of **3c**-bound HIV-1 protease revealed a number of important molecular insights into the ligand-binding site interactions.

© 2012 Elsevier Ltd. All rights reserved.

HIV-1 protease inhibitors continue to be a critical component of frontline therapy in the treatment of HIV patients.<sup>1–3</sup> Our continuing studies on the structure-based design of inhibitors targeting the protein backbone led to the discovery of a variety of novel HIV-1 protease inhibitors (PIs) with broad-spectrum activity against multidrug-resistant HIV-1 variants.<sup>4–8</sup> We recently reported various C3-functionalized cyclopentyltetrahydrofuran (Cp-THF)-derived P2-ligands designed to specifically interact with the flap Gly48 amide NH in the S2-subsite of the HIV-1 protease.<sup>9</sup> One of these inhibitors, **2** (Fig. 1), containing a 3-(*R*)-hydroxy group on the Cp-THF core displayed exceptionally potent enzyme inhibitory ( $K_i$  = 5 pM) and antiviral activity ( $IC_{50}$  = 2.9 nM). This inhibitor also exhibited potent activity against a panel of multidrug-resistant HIV-1 variants. The X-ray crystal structure of **2**-bound HIV protease revealed an extensive hydrogen-bonding network with the enzyme backbone.<sup>9</sup> Of particular interest, the 3-(*R*)-hydroxy group of the Cp-THF ligand was involved in an interesting water-mediated interaction with the backbone NH amide bond of Gly48. This specific interaction was not present in inhibitor **1**. These additional interactions observed with **2** may have contributed toward its impressive drug resistance profile.<sup>9</sup>

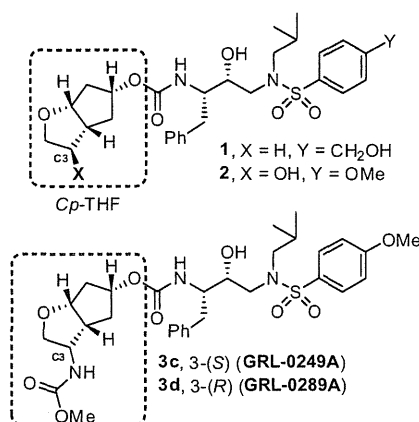
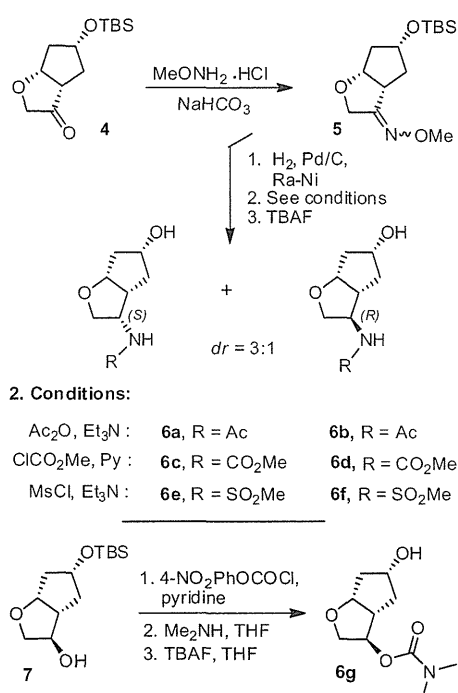
Based upon the **2**-bound X-ray crystal structure of HIV-1 protease, and given the significant gain in antiviral activity observed

with the addition of C3-polar substituents on the Cp-THF P2 ligand, we subsequently speculated that N-substituted functionalities, particularly *N*-acyl, *N*-carbamate or *N*-sulfonyl derivatives could function as both a hydrogen-bonding donor and acceptor. The NH proton could conceivably form an effective hydrogen bond with the proximal Gly48 carbonyl while amide or urethane carbonyl oxygen may form an additional interaction with the protease backbone. Indeed, our previous exploration of such hydrogen bond donor and acceptor functionalities on P2-ligand frameworks led to remarkably potent HIV-1 protease inhibitors with broad-spectrum antiviral activity.<sup>4–9</sup> Herein, we report the design, synthesis and biological evaluation of a series of HIV-1 protease inhibitors with C-3 substituted Cp-THF as the P2-ligand. A number of inhibitors exhibited exceptionally potent antiviral activity against a panel of multidrug-resistant HIV-1 variants. A protein-ligand X-ray crystal structure also provided important molecular insight into the ligand-binding site interactions.

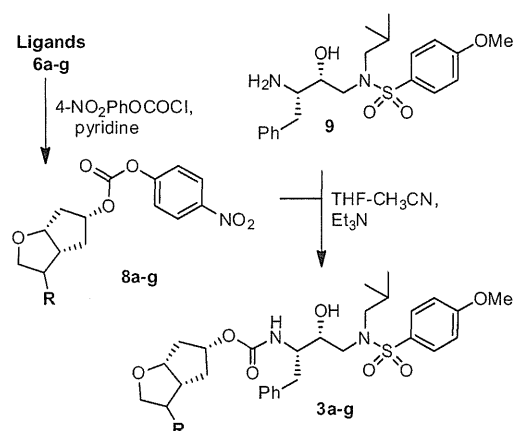
The synthesis of ligands containing various N-substituents with either stereochemistry at C3 was accomplished starting from our previously reported optically active ketone intermediate **4**<sup>10</sup> as shown in Scheme 1. Ketone **4** was converted to methyloxime derivatives **5** in 96% yield. Reduction of **5** with a mixture of Pd/C and Raney-Ni under hydrogen pressure (80 psi) provided the corresponding amine as a 3:1 diastereomeric mixture.<sup>11</sup> The amine mixture was reacted with Ac<sub>2</sub>O in the presence of Et<sub>3</sub>N and a catalytic amount of DMAP to yield a mixture of isomeric TBS-protected

\* Corresponding author. Tel.: +1 765 494 5323; fax: +1 765 496 1612.

E-mail address: [akghosh@purdue.edu](mailto:akghosh@purdue.edu) (A.K. Ghosh).

Figure 1. Structure of protease inhibitors **1**, **2**, **3c**–**d**.Scheme 1. Synthesis of C3-substituted ligands **6a**–**g**.

amide intermediates in 80% yield. Treatment of the respective amides with TBAF in THF and chromatographic separation furnished diastereomerically pure ligands **6a** and **6b** in excellent yield. Similarly, the amine mixture was treated with methyl chloroformate and pyridine, or mesyl chloride and Et<sub>3</sub>N to afford the corresponding carbamates and sulfonamides. Treatment of the respective crude mixtures with TBAF in THF followed by chromatographic separation afforded diastereoisomeric *N*-carbamate ligands **6c** and **6d**, and *N*-mesyl ligands **6e** and **6f**, respectively. The assignment of stereochemistry on the ligands was carried out by NOE or NOESY experiments of the corresponding mixed activated carbonates **8a**, **8c**, and **8e**. To probe the importance of the free NH, we have synthesized ligand **6g** containing a 3-(*R*)-*O*-dimethylaminocarbamate group. This was synthesized in three consecutive steps starting from our previously reported optically active alcohol **7**.<sup>9</sup> Treatment of **7** with 4-nitrophenyl chloroformate in the presence of pyridine furnished the corresponding mixed activated carbonate. The resulting carbonate was reacted with a bubbling stream of

Scheme 2. Synthesis of protease inhibitors **3a**–**g**.

Me<sub>2</sub>NH gas to provide the corresponding TBS-protected ligand. Removal of the TBS-group with TBAF furnished ligand **6g** in excellent yield.

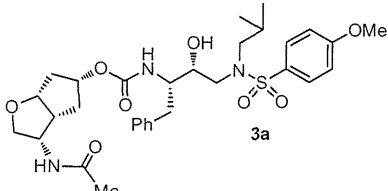
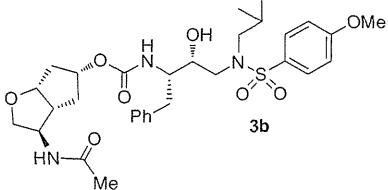
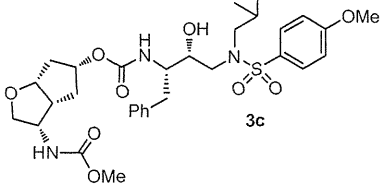
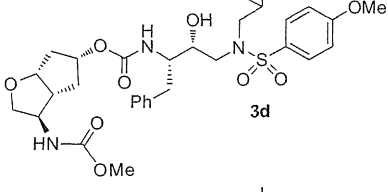
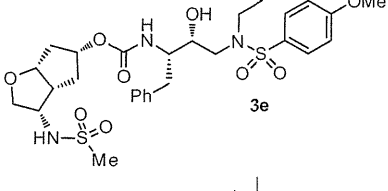
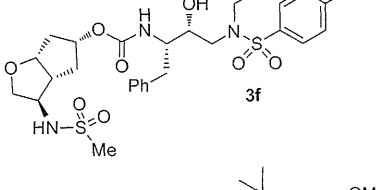
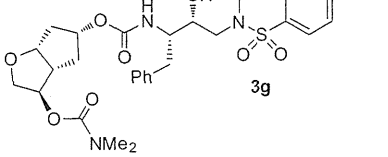
For the synthesis of HIV protease inhibitors, all ligand alcohols **6a**–**g** were reacted with 4-nitrophenyl chloroformate in the presence of pyridine in CH<sub>2</sub>Cl<sub>2</sub> to furnish the corresponding mixed activated carbonates **8a**–**g** (Scheme 2).<sup>9,10</sup> The activated carbonates were then reacted with previously reported hydroxyethylamine isostere **9** in the presence of Et<sub>3</sub>N in THF/CH<sub>3</sub>CN for 2–4 days to give corresponding inhibitors **3a**–**g**.

Inhibitors **3a**–**g** were initially tested in enzyme inhibitory assays using the method developed by Toth and Marshall,<sup>12</sup> and then evaluated for in vitro antiviral assays. Results are shown in Table 1. All inhibitors displayed impressive inhibitory potency and high antiviral activity. Inhibitors **3a** and **3b** that contain a 3-(*S*)- or 3-(*R*)-*N*-acetyl substituent on the Cp-THF ligand, exhibited similar potency (7.4 and 7.5 pM, respectively). Interestingly, the stereochemistry at C3 seemed to have little effect. Inhibitor **3c** with a 3-(*S*)-*N*-methoxycarbonyl displayed the most impressive enzyme and antiviral potency (*K*<sub>i</sub> = 1.8 pM and IC<sub>50</sub> = 1.6 nM). The isomeric inhibitor **3d** provided slightly lower potency. Inhibitors **3e** and **3f** that contain a 3-*N*-mesyl on the Cp-THF ligand, showed a substantial reduction in activity probably due to the increase in steric bulk created by the *N*-mesyl group. Inhibitor **3g** that contains an *O*-substituted dimethylaminocarbamate in place of *N*-substituted carbamate at C3 provided a good antiviral activity, similar to that of **3d**.

Inhibitors **3c** and **3d**, were further evaluated against a panel of multidrug-resistant (MDR) HIV-1 variants and their antiviral activities were compared to clinically available PI, darunavir (DRV).<sup>6,13</sup> Results are shown in Table 2. All inhibitors exhibited low nanomolar EC<sub>50</sub> values against the wild-type HIV-1<sub>ERS104pre</sub> laboratory strain, isolated from a drug-naïve patient.<sup>13</sup> Inhibitor **3d** had the most potent activity (EC<sub>50</sub> = 3 nM) similar to that of DRV. When tested against a panel of multidrug-resistant HIV-1 strains, the EC<sub>50</sub> of **3d** remained in the low nanomolar value range (15–24 nM) and its fold-changes in activity were similar to those observed with DRV.<sup>6,13</sup> Interestingly, inhibitor **3c**, with the opposite (*S*) stereochemistry at C3, displayed slightly lower antiviral activities against all viral strains compared to **3d**. However, the fold-changes in EC<sub>50</sub> for **3c** remained low (<3) against all MDR HIV-1 viruses. The fold-changes contrasted with those of **3d** and even DRV, for which the respective EC<sub>50</sub>'s increased by a factor of at least three against the MDR viruses examined.<sup>14</sup>

In order to gain molecular insights on the ligand-binding site interactions responsible for the potent activity and excellent resistance profile of **3c**, we have determined the X-ray crystal structure

**Table 1**  
Structures and potency of inhibitors **3a–g**<sup>a</sup>

Entry	Inhibitor structure	K <sub>i</sub> (pM)	IC <sub>50</sub> (nM) <sup>b</sup>
1		7.4	25
2		7.5	31
3		1.8	1.6
4		4.0	4.6
5		32	28
6		180	50
7		20	4.7

<sup>a</sup> Values are the mean value of at least two experiments.<sup>b</sup> Human T-lymphoid (MT-2) cells ( $2 \times 10^3$ ) were exposed to 100 TCID<sub>50</sub> of HIV-1<sub>LAI</sub> and cultured in the presence of each PI, and IC<sub>50</sub> values were determined using the MTT assay. The IC<sub>50</sub> values of amprenavir (APV), saquinavir (SQV), indinavir (IDV), and darunavir (DRV) were 0.03, 0.015, 0.03, and 0.003 μM, respectively.

of the HIV wild-type protease complexed with **3c** (Fig. 2).<sup>15</sup> The structure was refined to an R-factor of 14.9% and a resolution of

**Table 2**Comparison of the antiviral activity of **3c**, **3d**, and DRV against multidrug-resistant HIV-1 variants

Virus <sup>a</sup>	EC <sub>50</sub> (μM) ±SDs, (fold-change) <sup>b</sup>		
	<b>3c</b>	<b>3d</b>	DRV
HIV-1 <sub>ERS104pre</sub> (WT)	0.029 ± 0.002	0.003 ± 0.001	0.004 ± 0.001
HIV-1 <sub>MDR/B</sub> (X4)	0.075 ± 0.011 (3)	0.018 ± 0.003 (6)	0.019 ± 0.006 (5)
HIV-1 <sub>MDR/C</sub> (X4)	0.030 ± 0.006 (1)	0.015 ± 0.005 (5)	0.011 ± 0.003 (3)
HIV-1 <sub>MDR/G</sub> (X4)	0.039 ± 0.001 (1)	0.020 ± 0.005 (7)	0.011 ± 0.002 (3)
HIV-1 <sub>MDR/TM</sub> (X4)	0.074 ± 0.006 (3)	0.024 ± 0.004 (8)	0.028 ± 0.001 (7)

<sup>a</sup> Amino acid substitutions identified in the protease-encoding region of HIV-1<sub>ERS104pre</sub>, HIV-1<sub>MDR/B</sub>, HIV-1<sub>MDR/C</sub>, HIV-1<sub>MDR/G</sub>, HIV-1<sub>MDR/TM</sub> compared to the consensus type B sequence cited from the Los Alamos database include L63P in HIV-1<sub>ERS104pre</sub>; L10I, K14R, L33I, M36I, M46I, F53I, K55R, I62V, L63P, A71V, G73S, V82A, L90M, I93L in HIV-1<sub>MDR/B</sub>; L10I, I15V, K20R, L24I, M36I, M46I, I54V, I62V, L63P, K70Q, V82A, and L89M in HIV-1<sub>MDR/C</sub>; L10I, V11I, T12E, I15V, L19I, R41K, M46I, L63P, A71T, V82A, and L90M in HIV-1<sub>MDR/G</sub>; L10I, K14R, R41K, M46I, I54V, L63P, A71V, V82A, L90M, I93L in HIV-1<sub>MDR/TM</sub>. HIV-1<sub>ERS104pre</sub> served as a source of wild-type HIV-1.

<sup>b</sup> EC<sub>50</sub> values were determined by using PHA-PBMs as target cells and the inhibition of p24 Gag protein production for each drug was used as an endpoint. The numbers in parentheses represent the fold-change in EC<sub>50</sub> values for each isolate compared to the EC<sub>50</sub> values for the wild-type HIV-1<sub>ERS104pre</sub>. All assays were conducted in duplicate, and the data shown represent mean values (±1 standard deviations) derived from the results of two or three independent experiments. PHA-PBMs were derived from a single donor in each independent experiment. DRV (darunavir).

1.23 Å. The inhibitor is bound to the protease dimer in two orientations related by a 180° rotation, with a 50/50 relative occupancy. The protease backbone structure showed a very low rms deviation of 0.11 Å for all Cα carbons compared to the protease complexes of **2**<sup>9</sup> or DRV.<sup>21</sup> As shown in Figure 2, the inhibitor interactions in the protease binding site extend from S2 to S2' protease subsites and consist of a series of strong hydrogen bonds and weaker C–H...O and C–H...π interactions similar to those previously described for DRV,<sup>21</sup> or inhibitor **2**.<sup>9</sup> The Cp-THF cyclic oxygen forms a strong hydrogen bond with the backbone amide NH of Asp29 in the protease S2-binding site, similar to that previously observed with other Cp-THF-based inhibitors **1**<sup>5</sup> and **2**.<sup>9</sup> Critical differences, however, are observed with the additional interactions that the 3-(S)-N-methoxycarbonyl amino substituent on the Cp-THF makes throughout the S2–S3 subsites. As shown in Figure 2, the carbamate NH forms a strong hydrogen bond with the Gly48 backbone carbonyl. The carbamate carbonyl is observed to interact with the Arg8' guanidine side chain through a conserved water molecule. The methyl of the methoxy group then fits within the S3-hydrophobic pocket. The C3-N-methoxycarbonyl amino group creates a network of tight hydrogen bonds that literally links the protease flap region to the S2–S3 subsites' dimer interface. These new interactions and enthalpic nature of the additional hydrogen bonding created by the P2-ligand may certainly exert an enhanced anchoring effect of the inhibitor into the S2-subsite and further stabilize the closed conformation of the protease–ligand complex.

In conclusion, we have reported the structure-based design of a series of highly potent HIV-1 protease inhibitors incorporating C3-substituted cyclopentyltetrahydrofuran urethanes as P2-ligands. Various C3-N-substituents were investigated in order to create multiple interactions in the S2-subsite of the protease and specifically with the protease flap region. Inhibitors **3c** and **3d** displayed remarkable inhibitory potency and antiviral activity. When tested against a panel of MDR HIV-1 strains, inhibitor **3d**, with a 3-(R)-methoxycarbonyl on the Cp-THF ligand, provided the most impressive EC<sub>50</sub>s and fold-changes in activity which are comparable to those observed with clinically available DRV. Isomeric inhibitor **3c** displayed lower antiviral activity. However, it exhibited strikingly low fold-changes of antiviral activity when tested against MDR HIV-1 viruses. An X-ray crystal structure of the protease–**3c**

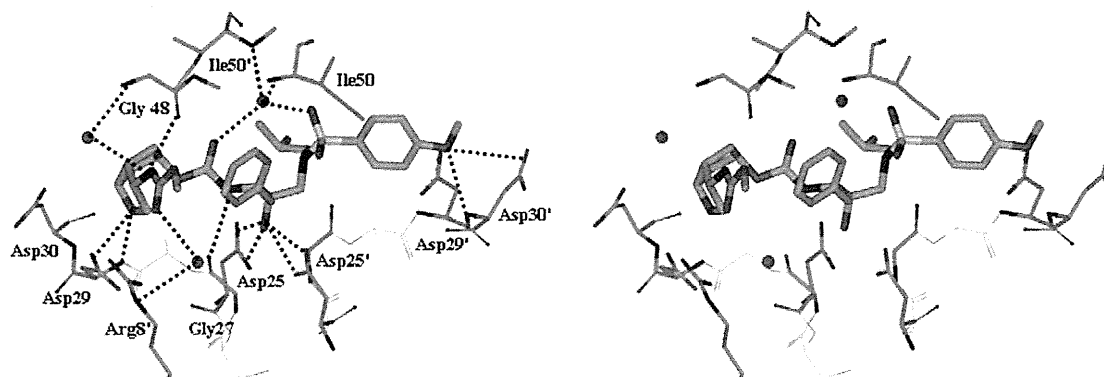


**Figure 2.** Stereoview of the X-ray structure of inhibitor **3c** (green)-bound HIV-1 protease (PDB code: 4DFG). All strong hydrogen bonding interactions are shown as dotted lines.

complex was determined at a 1.23 Å resolution. Inhibitor **3c** made extensive interactions throughout the protease binding site. The complex network of hydrogen-bonding interactions created by the *N*-methyl carbamate substituent in addition to those created by the isostere in the protease active site may account for the impressive antiviral activity and superb resistance profile observed with inhibitor **3c**. Further designs along this line and ligand optimization are currently underway.

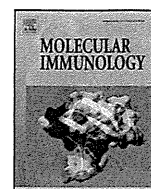
### Acknowledgements

This research was supported by the National Institutes of Health (Grant GM53386 to A.K.G. and Grant GM62920 to I.T.W.). This work was also supported by the Intramural Research Program of the Center for Cancer Research, National Cancer Institute, National Institutes of Health, and in part by a Grant-in-Aid for Scientific Research (Priority Areas) from the Ministry of Education, Culture, Sports, Science, and Technology of Japan (Monbu Kagakusho), a Grant for Promotion of AIDS Research from the Ministry of Health, Welfare, and Labor of Japan, and the Grant to the Cooperative Research Project on Clinical and Epidemiological Studies of Emerging and Reemerging Infectious Diseases (Renkei Jigyo) of Monbu-Kagakusho.

### References and notes

- Conway, B. *Future Virol.* **2009**, *4*, 39.
- Hue, S.; Gifford, R. J.; Dunn, D.; Fernhill, E.; Pillay, D. J. *Virol.* **2009**, *83*, 2645.
- Little, S. J.; Holte, S.; Routy, J. P.; Daar, E. S.; Markowitz, M.; Collier, A. C.; Koup, R. A.; Mellors, J. W.; Connick, E.; Conway, B.; Kilby, M.; Wang, L.; Whitcomb, J. M.; Hellmann, N. S.; Richman, D. D. *N. Engl. J. Med.* **2002**, *347*, 385.
- Ghosh, A. K. *J. Med. Chem.* **2009**, *52*, 2163.
- Ghosh, A. K.; Sridhar, P. R.; Leshchenko, S.; Hussain, A. K.; Li, J.; Kovalevsky, A. Y.; Walters, D. E.; Wedekind, J. E.; Grum-Tokars, V.; Das, D.; Koh, Y.; Maeda, K.; Gatanaga, H.; Weber, I. T.; Mitsuya, H. *J. Med. Chem.* **2006**, *49*, 5252.
- Ghosh, A. K.; Dawson, Z. L.; Mitsuya, H. *Bioorg. Med. Chem. Lett.* **2007**, *15*, 7576.
- Ghosh, A. K.; Leshchenko-Yashchuk, S.; Anderson, D. D.; Baldrige, A.; Noetzel, M.; Miller, H. B.; Tie, Y. F.; Wang, Y. F.; Koh, Y.; Weber, I. T.; Mitsuya, H. *J. Med. Chem.* **2009**, *52*, 3902.
- Ghosh, A. K.; Chapsal, B. D.; Weber, I. T.; Mitsuya, H. *Acc. Chem. Res.* **2008**, *41*, 78.
- Ghosh, A. K.; Chapsal, B. D.; Parham, G. L.; Steffey, M.; Agniswamy, J.; Wang, Y.-F.; Amano, M.; Weber, I. T.; Mitsuya, H. *J. Med. Chem.* **2011**, *54*, 5890.
- Ghosh, A. K.; Chapsal, B. D.; Baldrige, A.; Ide, K.; Koh, Y.; Mitsuya, H. *Org. Lett.* **2008**, *10*, 5135.
- Li, J. J.; Sutton, J. C.; Nirschl, A.; Zou, Y.; Wang, H.; Sun, C.; Pi, Z.; Johnson, R.; Krystek, S. R.; Seethala, R.; Golla, R.; Sleph, P. G.; Beehler, B. C.; Grover, G. J.; Fura, A.; Vyas, V. P.; Li, C. Y.; Gougoutas, J. Z.; Galella, M. A.; Zahler, R.; Ostrowski, J.; Hamann, L. G. *J. Med. Chem.* **2007**, *50*, 3015.
- Toth, M. V.; Marshall, G. R. *Int. J. Pept. Protein Res.* **1990**, *36*, 544.
- Koh, Y.; Nakata, H.; Maeda, K.; Ogata, H.; Bilcer, G.; Devasamudram, T.; Kincaid, J. F.; Boross, P.; Wang, Y.-F.; Tie, Y.; Volarath, P.; Gaddis, L.; Harrison, R. W.; Weber, I. T.; Ghosh, A. K.; Mitsuya, H. *Antimicrob. Agents Chemother.* **2003**, *47*, 3123.
- Ghosh, A. K.; Chapsal, B. Mitsuya, H. In *Aspartic Acid Proteases as Therapeutic Targets*; Ghosh, A., Ed.; Wiley-VCH Verlag GmbH & Co. KGaA: Weinheim, 2010; pp 245–262.
- The protein-ligand X-ray structure of **3c**-bound HIV-1 protease will be deposited in PDB (PDB ID: 4DFG). The HIV-1 protease was expressed and purified as previously described.<sup>16</sup> The protease-inhibitor complex was crystallized at room temperature by the hanging drop vapor diffusion method with well solutions of 1.2 M ammonium chloride and 0.1 M sodium acetate buffer (pH 4.8). Diffraction data were collected on a single crystal cooled to 90 K at SER-CAT BM beamline 22, Advanced Photon Source, Argonne National Laboratory (Chicago, IL, U.S.), with an X-ray wavelength of 1.0 Å and processed by HKL-2000 with  $R_{\text{merge}}$  of 7.2%. The PR structure was used in molecular replacement by PHASER<sup>17</sup> in the CCP4i suite<sup>18</sup> and refined to 1.45 Å resolution using SHELX-97 and COOT<sup>19</sup> for manual modification. PRODRG-2<sup>20</sup> was used to construct the inhibitor and the restraints for refinement. Alternative conformations were modeled, anisotropic atomic displacement parameters (*B* factors) were applied for all atoms including solvent molecules, and hydrogen atoms were added in the final round of refinement. The final refined solvent structure comprised two Cl<sup>−</sup> ions and 142 water molecules.
- Mahalingam, B.; Louis, J. M.; Hung, J.; Harrison, R. W.; Weber, I. T. *Proteins* **2001**, *43*, 455.
- Shen, C.-H.; Wang, Y.-F.; Kovalevsky, A. Y.; Harrison, R. W.; Weber, I. T. *FEBS J.* **2010**, *277*, 3699.
- Potterton, E.; Briggs, P.; Turkenburg, M.; Dodson, E. A. *Acta Crystallogr. Sect. D: Bio. Crystallogr.* **2003**, *59*, 1131.
- Emsley, P.; Cowtan, K. *Sect. D: Bio. Crystallogr.* **2004**, *60*, 2126.
- Schüttelkopf, A. W.; van Aalten, D. M. F. *Acta Crystallogr. Sect. D: Bio. Crystallogr.* **2004**, *60*, 1355.
- Kovalevsky, A. Y.; Liu, F.; Leshchenko, S.; Ghosh, A. K.; Louis, J. M.; Harrison, R. W.; Weber, I. T. *J. Mol. Biol.* **2006**, *363*, 161.





## Structural and functional mosaic nature of MHC class I molecules in their peptide-free form

Eiji Kurimoto<sup>a,b</sup>, Kimiko Kuroki<sup>c</sup>, Yoshiki Yamaguchi<sup>a,d</sup>, Maho Yagi-Utsumi<sup>a,e</sup>, Takahiro Igaki<sup>a</sup>, Takeshi Iguchi<sup>f</sup>, Katsumi Maenaka<sup>c,g</sup>, Koichi Kato<sup>a,e,\*</sup>

<sup>a</sup> Graduate School and Faculty of Pharmaceutical Sciences, Nagoya City University, Nagoya 467-8603, Japan

<sup>b</sup> Faculty of Pharmacy, Meijo University, Nagoya 468-8503, Japan

<sup>c</sup> Faculty of Pharmaceutical Sciences, Hokkaido University, Sapporo 060-0812, Japan

<sup>d</sup> RIKEN, Advanced Science Institute, Chemical Biology Department, Systems Glycobiology Research Group, Structural Glycobiology Team, Wako, Saitama 351-0198, Japan

<sup>e</sup> Institute for Molecular Science and Okazaki Institute for Integrative Bioscience, National Institutes of Natural Sciences, Okazaki 444-8787, Japan

<sup>f</sup> Bioscience Research Laboratory, Fujiya Co. Ltd., Hadano, Kanagawa 257-0031, Japan

<sup>g</sup> CREST, Japan Science and Technology Agency, Saitama, Japan

### ARTICLE INFO

#### Article history:

Received 18 January 2013

Received in revised form 14 March 2013

Accepted 15 March 2013

Available online 8 April 2013

#### Keywords:

MHC class I

Peptide-free form

$\beta_2$  microglobulin

NMR

NK cell receptors

Refolding

### ABSTRACT

Despite well-organized peptide-loading mechanisms within the endoplasmic reticulum, major histocompatibility complex class I (MHC-I) molecules can be displayed on cell surfaces in peptide-free forms. Although these empty MHC-I (eMHC-I) molecules are presumably involved in physiological and pathological processes, little is known about their structures and functions due to their instability. Using bacterially expressed HLA-Cw\*07:02 heavy chain and  $\beta_2$  microglobulin molecules, we successfully established an *in vitro* refolding method to prepare eMHC-I molecules in sufficient quantities for detailed structural analyses. NMR spectroscopy in conjunction with subunit-specific <sup>15</sup>N-labeling techniques revealed that the peptide-binding domains and the adjacent regions were unstructured in the peptide-free form, while the remaining regions maintained their structural integrity. Consistent with our spectroscopic data, the eMHC-I complex could interact with leukocyte Ig-like receptor B1, but not with killer cell Ig-like receptor 2DL3. Thus, eMHC-I molecules have a mosaic nature in terms of their three-dimensional structure and binding to immunologically relevant molecules.

© 2013 Elsevier Ltd. All rights reserved.

### 1. Introduction

Major histocompatibility complex class I (MHC-I) molecules are key proteins in the adaptive immune system as they bind endogenous antigenic peptides in the endoplasmic reticulum (ER) and subsequently present these to CD8<sup>+</sup> T lymphocytes at their cell surfaces (Saunders and van Endert, 2011). The maturation of MHC-I molecules is initiated by the formation of hetero-dimeric

complexes of membrane-bound heavy chains (HCs) consisting of  $\alpha 1$ ,  $\alpha 2$ , and  $\alpha 3$  domains and a light chain,  $\beta_2$  microglobulin ( $\beta_2m$ ). The subsequent peptide loading onto MHC-I molecules within the ER consists of multiple steps involving the molecular chaperone calreticulin, the thiol oxidoreductase Erp57, the peptide transporter associated with antigen processing (TAP), and the type I transmembrane glycoprotein tapasin (Paulsson and Wang, 2003; Wearsch and Cresswell, 2008).

Thus, these ER luminal proteins form peptide-loading complexes that capture empty MHC-I (eMHC-I) molecules, thereby stabilizing their states in order to bind endogenously processed peptides transported by TAP. Peptide-loaded MHC-I (pMHC-I) molecules are released and translocated via the Golgi apparatus to cell surfaces where they interact with T cell receptors on the membranes of MHC-I-restricted CD8<sup>+</sup> T lymphocytes and natural killer (NK) cell receptors, including leukocyte Ig-like receptors (LILRs) and killer cell Ig-like receptors (KIRs).

Despite these peptide-loading mechanisms within the ER, eMHC-I molecules can be displayed on cell surfaces under certain conditions and are possibly involved in some biological functions (Ortiz-Navarrete and Hämmerling, 1991; Theodossis, 2013). For

**Abbreviations:**  $\beta_2m$ ,  $\beta_2$  microglobulin; CD, circular dichroism; eMHC-I, empty MHC-I; ER, endoplasmic reticulum; GSH, glutathione; GSSG, glutathione disulfide; HC, heavy chain; HSQC, heteronuclear single-quantum coherence; KIRs, killer cell Ig-like receptors; LILRs, leukocyte Ig-like receptors; mAb, monoclonal antibody; MHC-I, major histocompatibility complex class I; NK, natural killer; NMR, nuclear magnetic resonance; pMHC-I, peptide-loaded MHC-I; SPR, surface plasmon resonance; TAP, transporter associated with antigen processing; TROSY, transverse relaxation-optimized spectroscopy.

\* Corresponding author at: Okazaki Institute for Integrative Bioscience, National Institutes of Natural Sciences, 5-1 Higashiyama, Myodaiji, Okazaki 444-8787, Japan. Tel.: +81 564 59 5225; fax: +81 564 59 5224.

E-mail address: [kkatonmr@ims.jp](mailto:kkatonmr@ims.jp) (K. Kato).

example, the NK inhibitory receptor Ly49C reportedly induced inhibitory signals upon interactions with eMHC-I molecules (Benoit et al., 2005). eMHC-I molecules were first identified on the surfaces of the TAP-deficient cell line RMA-S at low temperature (Ljunggren et al., 1990). eMHC-I molecules could bind exogenously added antigen peptides and subsequently underwent conformational transitions coupled with their stabilization (Elliott et al., 1991; Fahnestock et al., 1992; Schumacher et al., 1990). Furthermore, increasing evidence indicates that proliferating lymphoid cells exhibit a heterogeneous pool of MHC-I HCs at their cell surfaces that lack peptides and/or  $\beta_2m$  molecules. These are derived from fully mature pMHC-I molecules and are involved in both *cis* and *trans* interactions with various receptor molecules, including those for insulin, epidermal growth factor, and interleukin 2 (Arosa et al., 2007).

The three-dimensional structures of MHC-I molecules have been extensively studied in their peptide-loaded states (Bjorkman et al., 1987; Madden et al., 1991; Rudolph et al., 2006). However, only a few studies have attempted to elucidate the open conformations of eMHC-I (or HC) molecules, which included the non-classical MHC-I molecules HFE and M10 (Lebrón et al., 1998; Olson et al., 2005). Bouvier and Wiley characterized the peptide-free structures of MHC-I molecules with HLA-B7 HCs (B\*0702) by circular dichroism (CD) spectroscopy, fluorescence enhancement of hydrophobic probe, and limited proteolysis; these results indicated a molten globule-like nature of eMHC-I molecules (Bouvier and Wiley, 1998). Peptide-induced structural changes have also been characterized using several conformation-specific monoclonal antibodies (mAbs) (Hansen et al., 2005). In particular, mAb 64-3-7 that is specific for eMHC-I molecules defined a conformational change bearing its epitope located at a conserved  $\beta_{10}$ -helix-containing region of the  $\alpha 1$  domain (residues 46–52), which is close to the N-terminus of the peptide in a pMHC-I molecule and predicted to be exposed to solvent in the peptide-free state (Mage et al., 2012). To date, the atomic details for eMHC-I molecules have been provided by molecular dynamics simulations, which indicate conformational mobility of the  $\alpha 1/\alpha 2$  domains in eMHC-I molecules, particularly in the region that accommodates the peptide C-terminus (Zacharias and Springer, 2004).

In this study, we attempted to experimentally characterize eMHC-I conformations in solution using NMR spectroscopy. For this purpose, we established an *in vitro* refolding protocol to prepare recombinant eMHC-I complex from bacterially expressed HLA-Cw\*07:02 HC and  $\beta_2m$ . The structures of the MHC-I complex in solution were compared between peptide-free and -bound forms based on NMR spectroscopic data and binding activity with immune cell surface receptors.

## 2. Materials and methods

### 2.1. Protein expression

$\beta_2m$  and the extracellular region of HLA-Cw\*07:02 HC (residues 1–277) were each overexpressed in *Escherichia coli* BL21(DE3)-CodonPlus cells as inclusion bodies, which were solubilized using 6 M guanidinium chloride. Uniform and selective  $^{13}C/^{15}N$ -labeling methods were applied according to previously described protocols (Nishida et al., 2006; Yagi-Utsumi et al., 2011). To produce perdeuterated  $\beta_2m$  proteins, cells were grown in M9 minimal medium containing  $[^{15}N]NH_4Cl$  (1 g/L), uniformly  $^2H/^{13}C$ -labeled glucose (2 g/L), and  $^2H_2O$ . Solubilized  $\beta_2m$  was refolded by dialysis against 50 mM Tris–HCl buffer (pH 8.0) containing 1 M urea and 1 mM GSH/0.1 mM GSSG for 24 h at 16 °C, then against milli-Q water, and finally lyophilized. The DS11 nonapeptide (RYRPGTVAL) (Falk et al., 1993) was chemically synthesized by a solid phase method.

### 2.2. Reconstitution of pMHC-I molecules

The HC was denatured in 6 M guanidinium chloride (pH 2.2) for 30 min at room temperature, centrifuged to remove insoluble materials, and the resulting supernatant was slowly diluted 100-fold in ice-chilled reconstitution buffer consisting of 100 mM Tris–HCl (pH 8.0) that contained 400 mM L-arginine, 2 mM EDTA, 5 mM GSH, 0.5 mM GSSG, 10  $\mu$ M DS11, and 2  $\mu$ M refolded  $\beta_2m$ . After incubation for 48 h at 16 °C, the protein solution was concentrated with a Centrprep (Millipore YM-3), followed by gel filtration chromatography using a HiLoad 26/600 Superdex75pg column (GE Healthcare Life Sciences) equilibrated with 50 mM Tris–HCl (pH 8.0) at a flow rate of 1.2 ml/min. Purity of the refolding product was checked by SDS-PAGE.

### 2.3. Reconstitution of eMHC-I molecules

To produce the correctly folded eMHC-I complex in high yields, we prepared it from pMHC-I. The pMHC-I complex was denatured in 50 mM Tris–HCl (pH 8.0) containing 6 M guanidinium chloride for 30 min at room temperature, followed by gel filtration chromatography using an eluent consisting of 50 mM Tris–HCl (pH 8.0) and 6 M guanidinium chloride to isolate the HC with the correct disulfide bonds. Isolated HC was slowly diluted 50-fold in reconstitution buffer consisting of 400 mM L-arginine, 100 mM Tris–HCl (pH 8.0), 2 mM EDTA, and 3  $\mu$ M  $\beta_2m$ , followed by incubation for 24 h at 16 °C. eMHC-I complex was also purified by gel filtration as described above. Complete removal of the DS11 peptide from pMHC-I molecules was confirmed by reverse-phase HPLC using a Vydac C4 column (Grace Davison Discovery Sciences).

### 2.4. Surface plasmon resonance analysis

The extracellular domains (residues 1–200) of KIR2DL3 and the two N-terminal Ig-like domains (residues 1–197) of LILRB1 were prepared as described previously (Shiroishi 2003; Maenaka; 1999). Surface plasmon resonance (SPR) experiments used a BIAcore2000 system (GE Healthcare Life Sciences). Biotinylated HLA-Cw\*07:02 molecules, with and without the DS11 peptide and biotinylated bovine serum albumin as a negative control were immobilized on a research-grade CM5 chip (BIAcore) onto which streptavidin was covalently coupled. Soluble proteins dissolved in HBS-EP buffer (10 mM HEPES, pH 7.4, 150 mM NaCl, 3.4 mM EDTA, 0.005% surfactant P20) were injected over the chip at 25 °C. The binding response at each analyte concentration was calculated by subtracting the equilibrium response measured in the control flow cell from the response in the HLA-Cw\*07:02 flow cell. These data were analyzed using BIAevaluation 4.1 (GE Healthcare Life Sciences) and Origin 7 (Microcal, Northampton, MA) software. Equilibrium analysis determined  $K_d$  values by nonlinear curve fitting of a Langmuir binding isotherm.

### 2.5. CD and fluorescence measurements

CD spectra of eMHC-I and pMHC-I molecules at protein concentrations of 0.1–0.2 mg/ml in 50 mM Tris–HCl buffer (pH 8.0) were measured at 20 °C in a 1-mm quartz cuvette using a J-720 spectropolarimeter (JASCO, Tokyo). After subtracting a blank curve, the spectral data were presented as mean residue ellipticities. Secondary structure contents were calculated using reference sets determined by Yang et al. (1986). Fluorescence spectra of eMHC-I and pMHC-I molecules at protein concentrations of 0.01 mg/ml in 50 mM Tris–HCl buffer (pH 8.0) were measured using an FP-777 spectrofluorometer (JASCO) at 25 °C with an excitation wavelength of 280 nm.

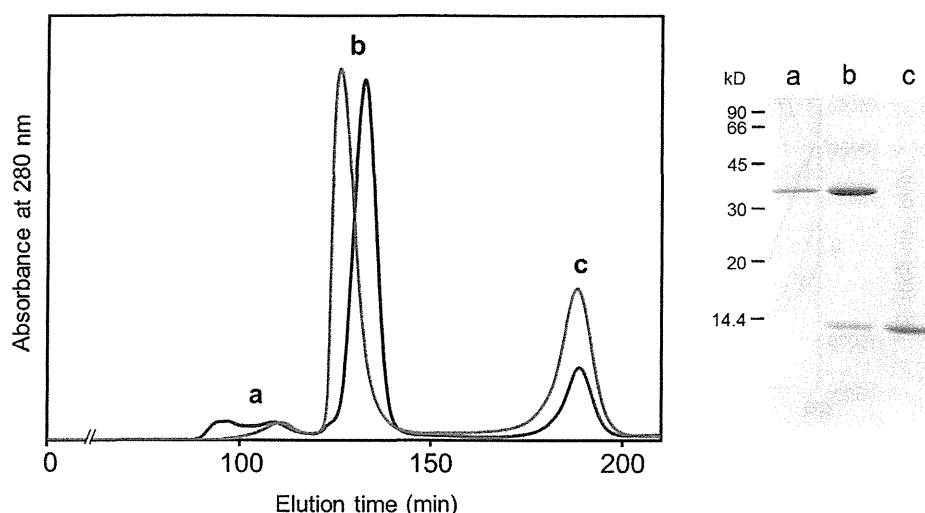


**Fig. 1.** Gel-filtration chromatograms of eMHC-I (red) and pMHC-I (blue). pMHC-I complexes were eluted in a fraction that corresponded to a molecular mass of 43 kDa, whereas eMHC-I molecules eluted in a 53-kDa fraction. SDS-PAGE gel of purified pMHC-I by gel filtration. Peaks: a, HC aggregates; b, MHC complexes; c, free  $\beta_2$ m.

## 2.6. NMR measurements

Proteins were dissolved at a concentration of up to 0.1 mM in 10 mM sodium phosphate buffer, pH 6.5, containing 10% (v/v)  $D_2O$ . NMR spectra were recorded at 30 °C using Bruker Avance-600 and JEOL ECA-920 spectrometers equipped with 5-mm triple-resonance probes, and a Bruker DMX-500 spectrometer equipped with a cryogenic probe. Spectral assignments were made by TROSY-based triple resonance experiments (HNCA, HN(CA)CO, HNCB, HN(CO)CA) (Pervushin et al., 1997; Tugarinov et al., 2004) and/or selective  $^{13}C$ – $^{15}N$  double labeling method (Kainosho and Tsuji, 1982).  $^1H$  chemical shifts were referenced to external 2,2-dimethyl-2-silapentane-5-sulfonic acid (DSS), while  $^{13}C$  and  $^{15}N$  chemical shifts were indirectly referenced to DSS by using absolute frequency ratios.

## 2.7. Three-dimensional structure model

The crystal structure of HLA-Cw3 (PDB code: 1EFX) (Boyington et al., 2000) was used as a template for the tertiary structure of HLA-Cw\*07:02. The SWISS-MODEL homology-modeling server (<http://www.swissmodel.expasy.org/>) was used to produce the homology coordinates (Arnold et al., 2006; Guex and Peitsch, 1997; Schwede et al., 2003) and PyMOL (<http://www.pymol.org/>) was used for viewing the outputs produced by the homology server.

## 3. Results and discussion

### 3.1. Preparation of eMHC-I molecules

Detailed structural analyses of eMHC-I molecules have thus far been hampered due to their structural instability (Silver et al., 1991; Theodossis, 2013). In this study, we attempted to establish a convenient protocol to prepare eMHC-I molecules in sufficient quantities for structural analyses. We utilized the HLA-Cw\*07:02 HC because we found this could form stable complexes with  $\beta_2$ m molecules in the absence of antigen peptides. By *in vitro* refolding, we successfully prepared eMHC-I molecules by combining  $\beta_2$ m molecules with HLA-Cw\*07:02 HCs, which were once correctly folded into pMHC-I complexes and subsequently isolated from the peptide under denaturing conditions.

The final yield of eMHC-I molecules from inclusion bodies was approximately 60%, which was suitable for structural analyses by NMR spectroscopy. Reverse-phase (RP) HPLC profile confirmed that eMHC-I was indeed free of the peptide (Supplementary Fig. S1). By gel-filtration chromatography, pMHC-I molecules were eluted as a peak at an elution time that corresponded to their molecular mass of 43 kDa, whereas eMHC-I molecules were eluted significantly faster than pMHC-I indicating its less compact structure in comparison with the peptide-free form (Fig. 1).

### 3.2. Overall structure of eMHC-I molecules

In their far-UV CD spectral data, pMHC-I molecules exhibited a deep trough at approximately 218 nm, a hallmark of a well-defined secondary structure, whereas eMHC-I molecules exhibited a comparatively shallower trough (Fig. 2A). Evaluation of these CD data indicated that the secondary structure of pMHC-I molecules consisted of 30%  $\alpha$ -helix and 60%  $\beta$ -strand conformations and the secondary structure of eMHC-I molecules comprised 9.5%  $\alpha$ -helix and 63%  $\beta$ -strand conformations. The  $\alpha$ -helices surrounding the peptide binding groove account for the great bulk of the  $\alpha$ -helical structure of pMHC-I. Therefore, the decreased intensity of CD signals was attributed to the breaking down of these helices. The fluorescence intensity of eMHC-I molecules decreased and showed a red-shift as compared with pMHC-I molecules (Fig. 2B), which suggested exposure of tryptophan residues coupled with disruption of the helical structures in the absence of the peptide. All of these data were consistent with previously reported physicochemical characterizations of the eMHC-I molecule that was formed from HLA-B\*0702 and  $\beta_2$ m subunits (Bouvier and Wiley, 1998).

Furthermore, we observed CD and fluorescence spectral change of eMHC-I upon addition of the DS11 peptide (Fig. 2). The data indicated that approximately 30% of eMHC-I form a complex with the peptide. The incomplete reconversion suggested that eMHC-I existed as minor peptide-receptive and major nonreceptive conformers that were separated by a high energy barrier. It is possible that the peptide-loading complexes in the ER accelerate formation of the peptide-receptive structure.

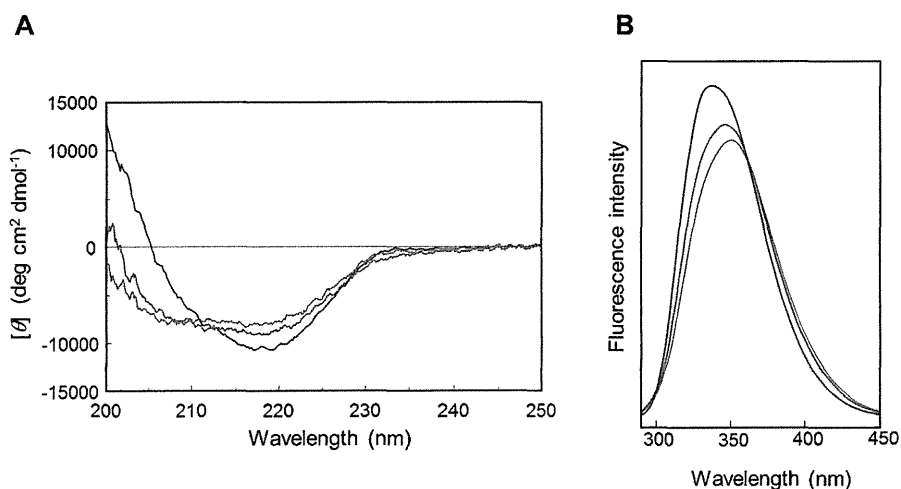


Fig. 2. (A) Far UV CD and (B) fluorescence spectra of eMHC-I complex (red), pMHC-I complex (blue), and eMHC-I complex with the DS11 peptide added afterward (green).

### 3.3. NMR analysis of eMHC-I molecules

For more detailed structural analyses, we measured NMR spectra of MHC complexes with subunit-selective <sup>15</sup>N-labeling. The eMHC-I complex formed from uniformly <sup>15</sup>N-labeled HC and non-labeled  $\beta_2m$  subunits gave an HSQC spectrum showing severe peak broadening and overlapping, which are hallmarks of non-native structures, as well as well-dispersed peaks that reflect folded conformations (Supplementary Fig. S2). This indicated that eMHC-I molecules contained both structured and unstructured regions. The peak broadening suggested some parts of eMHC-I underwent intermediate exchanges among multiple conformational states on the NMR chemical shift time scale as observed for proteins in molten-globule states (Schulman et al., 1997), although spectral assignments were difficult to make for these areas by conventional sequential assignment protocols. To provide site-specific information, we prepared the HC subunit labeled with <sup>15</sup>N specifically at methionine residues, which was complexed with unlabeled  $\beta_2m$  subunit (and the DS11 peptide). This pMHC-I complex showed three HSQC peaks originating from the three methionine residues in HC: Met5, Met98, and Met261 (Fig. 3). In the eMHC-I spectrum,

the peak intensities for Met5 and Met98 were markedly attenuated, although the Met261 peak intensity was constantly observed, which suggested structural integrity of the  $\alpha 3$  domain as compared with the remaining region.

Next, we compared the TROSY spectra of uniformly <sup>2</sup>H- and <sup>15</sup>N-labeled  $\beta_2m$  protein complexed with unlabeled HLA-Cw\*07:02 HC in both the peptide-bound and peptide-free states. The  $\beta_2m$  amino acid residues located at the interface with the  $\alpha 1/\alpha 2$  domains exhibited significant chemical shift differences between the eMHC-I and pMHC-I forms, while the remaining regions were minimally perturbed (Fig. 4 and Supplementary Table S1). Taken together, our NMR spectral data indicated that the  $\alpha 1/\alpha 2$  domains and their adjacent region were conformationally altered in the peptide-free form, while the three-dimensional structures of the remaining regions were insensitive to the presence or absence of the peptide.

A recently reported NMR study indicated that free  $\beta_2m$  exhibits line broadening due to conformational dynamics in the regions that are engaged in interaction with HCs (Hee et al., 2013). Furthermore, it was revealed that these regions become less flexible upon complex formation with HLA-B\*27:09 HC giving rise to pMHC-I. A similar tendency was observed in the present NMR data

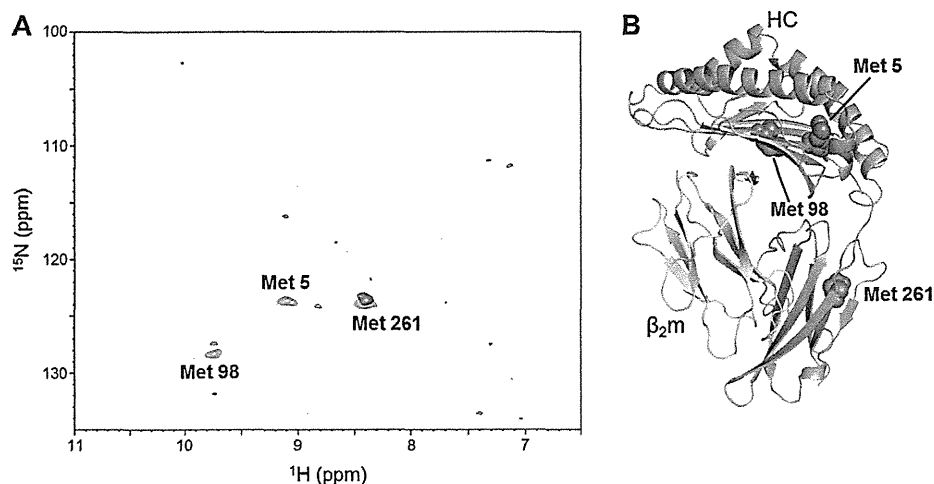
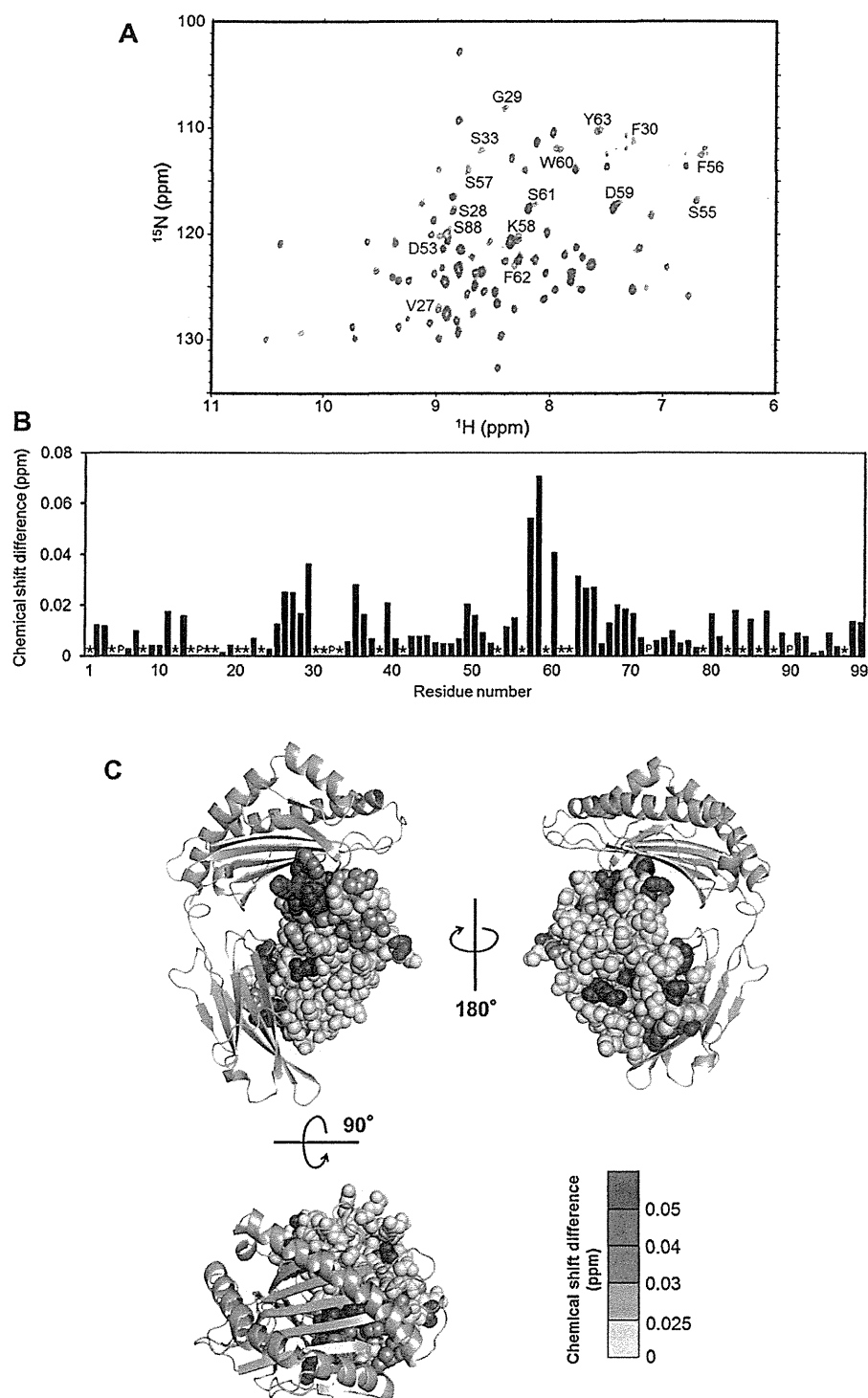


Fig. 3. (A) Superposition of <sup>1</sup>H-<sup>15</sup>N TROSY NMR spectra of eMHC-I (red) and pMHC-I (blue) molecules labeled with <sup>15</sup>N at the amide groups of methionine residues in HCs. The three methionine peaks were assigned by HNCO measurements combined with carbonyl <sup>13</sup>C-labeling of selected amino acid residues. Spectral reproducibility was confirmed by experiments using the amino acid-selective <sup>13</sup>C- and <sup>15</sup>N-double labeling method (data not shown) and (B) three-dimensional structure model of HLA-Cw\*07:02 based on the crystal structure of HLA-Cw3 (PDB code: 1EFX) indicating the residues used as spectroscopic probes.



**Fig. 4.** (A) Superposition of  $^1\text{H}$ - $^{15}\text{N}$  TROSY NMR spectra of uniformly  $^2\text{H}$ -,  $^{13}\text{C}$ - and  $^{15}\text{N}$ -labeled  $\beta_2\text{m}$  in the eMHC-I (red) and pMHC-I (blue) complexes. The spectral assignments for  $\beta_2\text{m}$  in the pMHC-I complex were made by TROSY-based HNCA, HN(CA)CO, HNCO, and HN(CO)CA. Spectral reproducibility was confirmed by experiments using a series of amino acid-selective  $^{15}\text{N}$ -labeling (data not shown). (B) Plots of the chemical shift differences of the backbone  $\beta_2\text{m}$  amide peaks [ $(0.04\Delta\delta_N^2 + \Delta\delta_H^2)^{1/2}$ , where  $\delta_N$  and  $\delta_H$  represent the difference in nitrogen and proton chemical shifts, respectively] between the eMHC-I and pMHC-I forms. Asterisk indicates an amino acid residue that did not exhibit an observable peak in eMHC-I and/or pMHC-I while "P" represents a proline residue. (C) Mapping of the chemical shift differences observed between eMHC-I and pMHC-I molecules on the three-dimensional structure model of HLA-Cw\*07:02. Red gradient indicates the degree of a chemical shift difference. The residues whose HSQC peak was observed in pMHC-I but undetectable due to line broadening in eMHC-I are shown in purple. Proline and unassigned residues are shown in gray.

(Supplementary Fig. 3 and Supplementary Tables S1 and S2). The conformational flexibility of  $\beta_2\text{m}$  could be interpreted as indicating its adaptability of diverse HCs. Moreover, our data revealed that the amino acid residues in these regions, especially those located in

the segment involved in contacts with the  $\alpha 1/\alpha 2$  domains, exhibited significant line broadening and/or chemical shift changes in the eMHC-I complex (Fig. 4 and Supplementary Table S1). These data suggest the  $\beta_2\text{m}$  segment at the interface with the  $\alpha 1/\alpha 2$  domains

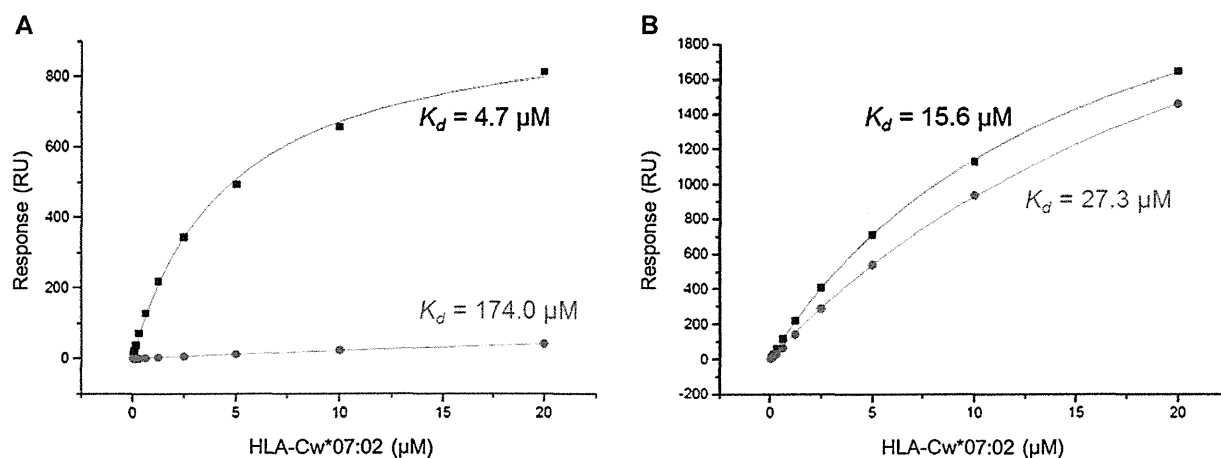


**Fig. 5.** SPR analyses of the interactions of biotinylated MHC-I [in peptide-free (red) and peptide-loaded (black) forms] with the extracellular domains of KIR2DL3 (A) and with the two N-terminal domains of LILRB1 (B).  $K_d$  values are as indicated.

has mobility in the peptide-free form. One intriguing possibility is that the  $\alpha 1/\alpha 2$  domains and its adjacent region in  $\beta_2\text{m}$  undergo conformational transition in a concerted fashion.

#### 3.4. Binding activity of eMHC-I molecules with immune cell surface receptors

The structural integrity of eMHC-I molecules was further probed using the MHC-I binding immune receptors LILRB1 and KIR2DL3. SPR data showed that the extracellular domains of KIR2DL3 had a much lower affinity for eMHC-I molecules as compared with pMHC-I molecules, whereas the two N-terminal Ig-like domains of LILRB1 had comparable affinities for both immune receptors (Fig. 5, Supplementary Fig. S4). The reduced binding of eMHC-I to KIR2DL3 could be explained by the structural disruption of its peptide-binding  $\alpha 1/\alpha 2$  domains, which also provide a KIR-adaptor site (Boyington et al., 2000; Fan et al., 2001). In contrast, the LILRB1-binding surface is provided by the  $\alpha 3$  domain and  $\beta_2\text{m}$  (Shiroishi et al., 2006; Willcox et al., 2003). Consistently, our NMR data demonstrated the structural integrity of the LILRB1-binding regions in eMHC-I molecules. These data again indicated that the absence of peptides caused structural alterations within limited regions of MHC-I molecules and that the remaining regions remained functionally intact.

#### 4. Conclusion

In the present study, we developed a stable-isotope-assisted NMR approach that was a useful tool for detailed structural characterizations of MHC-I molecules in both free and peptide-loaded forms. While previous reports have underscored structural disorders in the peptide-binding domains of eMHC-I molecules, our present data emphasize the mosaic nature of eMHC-I molecules in terms of their three-dimensional structures and binding to immunologically relevant molecules. These findings provide insights into the peptide-loading mechanisms and possible biological roles of MHC-I molecules in their peptide-free state.

#### Acknowledgements

We thank Dr. Hiroaki Sasakawa and Ms. Michiko Nakano (Institute for Molecular Science) their help with NMR measurements. We thank Ms. Kiyomi Senda and Ms. Kumiko Hattori (Nagoya City University) for their help with preparing recombinant proteins. This work was supported in part by the Nanotechnology Platform

Project and Grants-in-Aid for Scientific Research on Innovative Areas (20107004) and for Scientific Research (C) (16590032) and (A) (24249002) from the Ministry of Education, Culture, Sports, Science and Technology of Japan.

#### Appendix A. Supplementary data

Supplementary data associated with this article can be found, in the online version, at <http://dx.doi.org/10.1016/j.molimm.2013.03.014>.

#### References

- Arnold, K., Bordoli, L., Kopp, J., Schwede, T., 2006. The SWISS-MODEL workspace: a web-based environment for protein structure homology modelling. *Bioinformatics* 22, 195–201.
- Arosa, F.A., Santos, S.G., Powis, S.J., 2007. Open conformers: the hidden face of MHC-I molecules. *Trends in Immunology* 28, 115–123.
- Benoit, L.A., Shannon, J., Chamberlain, J.W., Miller, R.G., 2005. Influence of xenogeneic  $\beta_2$ -microglobulin on functional recognition of H-2K<sup>b</sup> by the NK cell inhibitory receptor Ly49C. *Journal of Immunology* 175, 3542–3553.
- Bjorkman, P.J., Saper, M.A., Samraoui, B., Bennett, W.S., Strominger, J.L., Wiley, D.C., 1987. Structure of the human class I histocompatibility antigen, HLA-A2. *Nature* 329, 506–512.
- Bouvier, M., Wiley, D.C., 1998. Structural characterization of a soluble and partially folded class I major histocompatibility heavy chain/ $\beta_2\text{m}$  heterodimer. *Nature Structural Biology* 5, 377–384.
- Boyington, J.C., Motyka, S.A., Schuck, P., Brooks, A.G., Sun, P.D., 2000. Crystal structure of an NK cell immunoglobulin-like receptor in complex with its class I MHC ligand. *Nature* 405, 537–543.
- Elliott, T., Cerundolo, V., Elvin, J., Townsend, A., 1991. Peptide-induced conformational change of the class I heavy chain. *Nature* 351, 402–406.
- Fahnestock, M.L., Tamir, I., Narhi, L., Bjorkman, P.J., 1992. Thermal stability comparison of purified empty and peptide-filled forms of a class I MHC molecule. *Science* 258, 1658–1662.
- Falk, K., Rotzschke, O., Grahovac, B., Schendel, D., Stevanovic, S., Gnau, V., Jung, G., Strominger, J.L., Rammensee, H.G., 1993. Allele-specific peptide ligand motifs of HLA-C molecules. *Proceedings of the National Academy of Sciences of the United States of America* 90, 12005–12009.
- Fan, Q.R., Long, E.O., Wiley, D.C., 2001. Crystal structure of the human natural killer cell inhibitory receptor KIR2DL1-HLA-Cw4 complex. *Nature Immunology* 2, 452–460.
- Guex, N., Peitsch, M.C., 1997. SWISS-MODEL and the Swiss-PdbViewer: an environment for comparative protein modeling. *Electrophoresis* 18, 2714–2723.
- Hansen, T.H., Lybarger, L., Yu, L., Mitaksov, V., Fremont, D.H., 2005. Recognition of open conformers of classical MHC by chaperones and monoclonal antibodies. *Immunological Reviews* 207, 100–111.
- Hee, C.S., Beerbaum, M., Loll, B., Ballasch, M., Schmieder, P., Uchanska-Ziegler, B., Ziegler, A., 2013. Dynamics of free versus complexed  $\beta_2$ -microglobulin and the evolution of interfaces in MHC class I molecules. *Immunogenetics* 65, 157–172.
- Kainosho, M., Tsuji, T., 1982. Assignment of the three methionyl carbonyl carbon resonances in streptomyces subtilisin inhibitor by a carbon-13 and nitrogen-15 double-labeling technique. A new strategy for structural studies of proteins in solution. *Biochemistry* 21, 6273–6279.

- Lebrón, J.A., Bennett, M.J., Vaughn, D.E., Chirino, A.J., Snow, P.M., Mintier, G.A., Feder, J.N., Bjorkman, P.J., 1998. Crystal structure of the hemochromatosis protein HFE and characterization of its interaction with transferrin receptor. *Cell* 93, 111–123.
- Ljunggren, H.G., Stam, N.J., Ohlén, C., Neefjes, J.J., Höglund, P., Heemels, M.T., Bastin, J., Schumacher, T.N., Townsend, A., Kärre, K., et al., 1990. Empty MHC class I molecules come out in the cold. *Nature* 346, 476–480.
- Madden, D.R., Gorga, J.C., Strominger, J.L., Wiley, D.C., 1991. The structure of HLA-B27 reveals nonamer self-peptides bound in an extended conformation. *Nature* 353, 321–325.
- Mage, M.G., Dolan, M.A., Wang, R., Boyd, L.F., Revilla, M.J., Robinson, H., Nataraajan, K., Myers, N.B., Hansen, T.H., Margulies, D.H., 2012. The peptide-receptive transition state of MHC class I molecules: insight from structure and molecular dynamics. *Journal of Immunology* 189, 1391–1399.
- Nishida, N., Motojima, F., Idota, M., Fujikawa, H., Yoshida, M., Shimada, I., Kato, K., 2006. Probing dynamics and conformational change of the GroEL–GroES complex by  $^{13}\text{C}$  NMR spectroscopy. *Journal of Biochemistry* 140, 591–598.
- Olson, R., Huey-Tubman, K.E., Dulac, C., Bjorkman, P.J., 2005. Structure of a pheromone receptor-associated MHC molecule with an open and empty groove. *PLoS Biology* 3, e257.
- Ortiz-Navarrete, V., Hämmerling, G.J., 1991. Surface appearance and instability of empty H-2 class I molecules under physiological conditions. *Proceedings of the National Academy of Sciences of the United States of America* 88, 3594–3597.
- Paulsson, K., Wang, P., 2003. Chaperones and folding of MHC class I molecules in the endoplasmic reticulum. *Biochimica et Biophysica Acta* 1641, 1–12.
- Pervushin, K., Riek, R., Wider, G., Wüthrich, K., 1997. Attenuated T2 relaxation by mutual cancellation of dipole–dipole coupling and chemical shift anisotropy indicates an avenue to NMR structures of very large biological macromolecules in solution. *Proceedings of the National Academy of Sciences of the United States of America* 94, 12366–12371.
- Rudolph, M.G., Stanfield, R.L., Wilson, I.A., 2006. How TCRs bind MHCs, peptides, and coreceptors. *Annual Review of Immunology* 24, 419–466.
- Saunders, P.M., van Endert, P., 2011. Running the gauntlet: from peptide generation to antigen presentation by MHC class I. *Tissue Antigens* 78, 161–170.
- Schulman, B.A., Kim, P.S., Dobson, C.M., Redfield, C., 1997. A residue-specific NMR view of the non-cooperative unfolding of a molten globule. *Nature Structural Biology* 4, 630–634.
- Schumacher, T.N., Heemels, M.T., Neefjes, J.J., Kast, W.M., Melief, C.J., Ploegh, H.L., 1990. Direct binding of peptide to empty MHC class I molecules on intact cells and in vitro. *Cell* 62, 563–567.
- Schwede, T., Kopp, J., Guex, N., Peitsch, M.C., 2003. SWISS-MODEL: an automated protein homology-modeling server. *Nucleic Acids Research* 31, 3381–3385.
- Shiroishi, M., Kuroki, K., Rasubala, L., Tsumoto, K., Kumagai, I., Kurimoto, E., Kato, K., Kohda, D., Maenaka, K., 2006. Structural basis for recognition of the nonclassical MHC molecule HLA-G by the leukocyte Ig-like receptor B2 (LILRB2/LIR2/ILT4/CD85d). *Proceedings of the National Academy of Sciences of the United States of America* 103, 16412–16417.
- Silver, M.L., Parker, K.C., Wiley, D.C., 1991. Reconstitution by MHC-restricted peptides of HLA-A2 heavy chain with  $\beta_2$ -microglobulin, in vitro. *Nature* 350, 619–622.
- Theodossis, A., 2013. On the trail of empty MHC class-I. *Molecular Immunology* 55, 131–134.
- Tugarinov, V., Hwang, P.M., Kay, L.E., 2004. Nuclear magnetic resonance spectroscopy of high-molecular-weight proteins. *Annual Review of Biochemistry* 73, 107–146.
- Wearsch, P.A., Cresswell, P., 2008. The quality control of MHC class I peptide loading. *Current Opinion in Cell Biology* 20, 624–631.
- Willcox, B.E., Thomas, L.M., Bjorkman, P.J., 2003. Crystal structure of HLA-A2 bound to LIR-1, a host and viral major histocompatibility complex receptor. *Nature Immunology* 4, 913–919.
- Yagi-Utsumi, M., Matsuo, K., Yanagisawa, K., Gekko, K., Kato, K., 2011. Spectroscopic characterization of intermolecular interaction of amyloid  $\beta$  promoted on GM1 micelles. *International Journal of Alzheimer's Disease* 2011, 925073.
- Yang, J.T., Wu, C.S., Martinez, H.M., 1986. Calculation of protein conformation from circular dichroism. *Methods in Enzymology* 130, 208–269.
- Zacharias, M., Springer, S., 2004. Conformational flexibility of the MHC class I  $\alpha_1$ – $\alpha_2$  domain in peptide bound and free states: a molecular dynamics simulation study. *Biophysical Journal* 87, 2203–2214.



